Geochemical Journal, Vol. 54, pp. 351 to 363, 2020 doi:10.2343/geochemj.2.0606

Constraints on redox conditions in the Japan Sea in the last 47,000 years based on Mo and W as palaeoceanographic proxies

MAKOTO TSUJISAKA,[1]* SHINSUKE NISHIDA,[1] SHOTARO TAKANO,[1] MASAFUMI MURAYAMA[2] and YOSHIKI SOHRIN[1]

[1]Institute for Chemical Research, Kyoto University, Gokasho, Uji, Kyoto 611-0011, Japan
[2]Center for Advanced Marine Core Research, Kochi University, B200 Monobe, Nankoku, Kochi 783-8502, Japan

(*Received November 21, 2019; Accepted June 30, 2020*)

Both molybdenum (Mo) and tungsten (W) form soluble oxyanions in oxic seawater, whereas Mo forms insoluble thiomolybdate and W forms soluble thiotungstate in sulfidic seawater. Thus, concentrations and stable isotope ratios of Mo and W in sediments may fluctuate due to changes in redox conditions and can be used to estimate paleoenvironmental changes. The modern Japan Sea is oxic from the surface to the bottom, whereas deep water became anoxic several times from the late Pleistocene to the Holocene. Detailed information on redox conditions is still lacking. In this study, we analyzed a sediment core that was collected from offshore Iwanai, Hokkaido (43°22′36″ N, 140°04′10″ E, water depth 900 m). To the best of our knowledge, our study is the first to report stable isotope data of Mo and W in sediments of the Japan Sea. We observed maxima in the Mo concentration of up to 29 ppm in the sediment layers of 11–10 ka, 17–14 ka (the last glacial maximum), 31 ka, and 45 ka in accordance with the maxima of total sulfur, thereby indicating the deposition of thiomolybdate $MoO_xS_{4-x}^{2-}$ ($0 \le x \le 3$). δ^{98}Mo, however, was between –0.19 and 0.69‰ at these ages, suggesting that the H_2S concentration in bottom water never exceeded 11 μmol kg^{-1}. The concentration and isotopic ratio of W were relatively constant throughout the core; W = 1.2 ± 0.2 ppm and δ^{186}W = 0.03 ± 0.03‰ (ave ± sd). The authigenic Mo and W ratio, Mo_{auth}/W_{auth} (mol/mol), was 10.5 ± 7.3 except for the above four ages, supporting the control of Mn and Fe (oxyhydr)oxides on Mo_{auth} and W_{auth} under oxic conditions.

Keywords: molybdenum, tungsten, stable isotopes, Japan Sea, paleoceanography

INTRODUCTION

The modern Japan Sea is a semi-closed environment surrounded by shallow straits. The Japan Sea sediments are composed of alternating layers of dark and light colored clay that reflect Dansgaard-Oeschger cycles (Tada, 1995; Tada *et al.*, 1999). The formation of the dark layers is attributed to the increase in productivity in surface waters and the decrease in the oxygen content in sediments, which were affected by changes in sea levels and/or the East Asian monsoon (Oba *et al.*, 1991, 1995; Tada *et al.*, 1999). These environmental changes have been investigated through various proxies. Oba *et al.* (1991) and Oba *et al.* (1995) estimated the paleoenvironmental history of the Japan Sea caused by sea level changes over the last 85 ka by using proxies such as isotope ratios of oxygen and carbon as well as microfossil assemblages. Tada *et al.* (1999) estimated the change in redox conditions of bottom water using the ratio of organic carbon to sulfur (C_{org}/S) and estimated the change in properties of surface water using diatom fossil assemblages. After these early studies, palaeoceanographic studies of the Japan Sea were performed using sediment fabrics (Khim *et al.*, 2009; Watanabe *et al.*, 2007), radiolarians in sediment (Itaki *et al.*, 2003, 2004), and metal concentrations (Lim *et al.*, 2011; Minoura *et al.*, 2012). The concentration of molybdenum (Mo) in the sediments has also been studied extensively to constrain the redox conditions in bottom water (Crusius *et al.*, 1996, 1999; Khim *et al.*, 2012; Xu *et al.*, 2014; Zou *et al.*, 2012).

Molybdenum is a redox-sensitive element and has seven stable isotopes (^{92}Mo, ^{94}Mo, ^{95}Mo, ^{96}Mo, ^{97}Mo, ^{98}Mo, and ^{100}Mo). In the modern ocean, Mo exists as an oxoacid anion of MoO_4^{2-} and is distributed homogeneously (Mo = 107 ± 7 nmol kg^{-1} and δ^{98}Mo = 2.34 ± 0.10‰, ave ± sd; (Nakagawa *et al.*, 2012) with a long residence time of 740,000 y (Firdaus *et al.*, 2008). The primary sink of Mo in the oxic ocean is the adsorption onto Mn and Fe (oxyhydr)oxides, and lighter isotopes of Mo are preferentially adsorbed, thereby resulting in isotopic fractionation (Barling *et al.*, 2001; Goldberg *et al.*, 2009). In sulfidic seawater, Mo forms particle-reactive

*Corresponding author (e-mail: tsujisaka.makoto.t93@kyoto-u.jp)

thiomolybdate anions of $MoO_xS_{4-x}^{2-}$ ($0 \le x \le 3$) via reaction with H_2S (Helz *et al.*, 1996). When the H_2S concentration becomes higher than 11 μmol kg^{-1}, most of Mo in seawater is transformed into thiomolybdate anions and fixed with organic matter and/or iron sulfides in sediments (Erickson and Helz, 2000). As a result, euxinic sediments and sulfide minerals have δ^{98}Mo values of 1.5–2.3‰, which are close to those of seawater (Dahl *et al.*, 2010; Neubert *et al.*, 2008; Poulson-Brucker *et al.*, 2009; Scott and Lyons, 2012). Thus, the concentrations and isotope ratios of Mo in sediments have been widely utilized as a redox proxy in paleoceanography (Calvert and Pedersen, 1993; Crusius *et al.*, 1996, 1999; Dahl and Wirth, 2017; Kendall *et al.*, 2011; Kurzweil *et al.*, 2016; Ostrander *et al.*, 2019; Thoby *et al.*, 2019; Wille *et al.*, 2008).

Like Mo, tungsten (W) belongs to Group 6 in the periodic table and has five stable isotopes (^{180}W, ^{182}W, ^{183}W, ^{184}W, and ^{186}W). In the modern ocean, W exists as the oxoacid anion WO_4^{2-} and is uniformly distributed with a concentration of 49 pmol kg^{-1} and an oceanic residence time of 14,000 y (Firdaus *et al.*, 2008; Sohrin *et al.*, 1987). In the East China Sea and the Yellow Sea, we found that W is released from continental shelf sediments when manganese reduction occurs, whereas Mo behaves conservatively (Sohrin *et al.*, 1999). Hence, we expected that the Mo/W concentration ratio in sediments would be a proxy for redox conditions due to the different behaviors of these elements. Unlike Mo, W is transformed into thiotungstate anions of $WO_xS_{4-x}^{2-}$ ($0 \le x \le 3$) only when the H_2S concentration increases above 60 μmol kg^{-1} and the thiotungstate is not particle-reactive (Mohajerin *et al.*, 2014, 2016). The partition coefficient of Mo between sediments and porewater increases with the H_2S concentration, but that of W is not affected by the H_2S concentration in a sediment core collected from the Izena Hole, where hydrothermal activities were observed (Watanabe *et al.*, 2017). Dissimilar behaviors of W and Mo have also observed in the Bothnian Bay during freshwater transport and estuarine mixing (Bauer *et al.*, 2018) and in hypoxic-euxinic marine basins in the Black Sea and the Baltic Sea (Dellwig *et al.*, 2019). Moreover, we have found that the concentration of W becomes extremely high (0.12–127 nmol kg^{-1}) in submarine hydrothermal fluids (Kishida *et al.*, 2004) and in the coastal seawater off large cites (Sohrin *et al.*, 1999). Recent studies revealed that δ^{186}W varies in geological materials: e.g., 0–0.08‰ for igneous rocks, 0–0.15‰ for manganese nodules, and 0–0.25‰ for marine sediments (Irisawa and Hirata, 2006; Krabbe *et al.*, 2017; Kurzweil *et al.*, 2018, 2019; Tsujisaka *et al.*, 2019). Hence, we expect that the concentration and isotopic composition of W would be a new proxy for assessing the contributions from lithogenic, hydrothermal, and anthropogenic sources.

For these reasons, the concentrations and isotope ratios of Mo and W in sediment cores will enable us to constrain the paleoceanographic conditions more precisely. However, there have been no reports of paleoceanographic study using all the concentrations and isotope ratios of Mo and W. Furthermore, there have been no reports of Mo isotope ratios, W concentrations, and W isotope ratios in the Japan Sea sediment core so far. In this study, we analyzed the sediment core IWANAI No. 3 collected from an intermediate depth of the northern Japan Sea off Iwanai, Hokkaido (43°22′36″ N, 140°04′10″ E, water depth 900 m). We report the concentration and isotopic composition of Mo and W along with the concentrations of major elements, including Al, Fe, Ca, C, S, Ti, and N, and trace elements such as Mn, P, Cr, Co, Ni, Cu, Zn, Cd, Sb, Ba, Tl, Bi, and U. We estimate environmental changes in the Japan Sea in the last 47,000 years and evaluate the possibility of Mo and W as new proxies for paleoceanography.

Materials and Methods

Site description

The modern Japan Sea is a semi-closed marginal sea with an area of approximately 1,000,000 km^2 and an average water depth of approximately 1,650 m (Menard and Smith, 1966), and it is surrounded by four shallow straits (Tsushima Strait, sill depth 130 m; Tsugaru Strait, 130 m; Soya Strait, 55 m; and Mamiya Strait, 18 m). Seawater from the open ocean flows into the Japan Sea mainly via the warm and high-salinity Tsushima Warm Current (TWC), which is a branch of the Kuroshio Current. Most of the TWC water flows out from the Tsugaru Strait to the Pacific Ocean as the Tsugaru Warm Current. The remaining water flows out from the Soya Strait to the Sea of Okhotsk as the Soya Warm Current (Toba, 1982). The Liman Current (LC), which originates from cold surface water in the Sea of Okhotsk and flows through the Mamiya Strait into the northern part of the Japan Sea. The Japan Sea Proper Water (JSPW) occurs below a water depth of 300–500 m and has an almost uniform temperature and salinity (Sudo, 1986). The JSPW is formed in the northwestern part of the Japan Sea by the subduction of high-density seawater due to strong cooling of the LC water in winter (Senjyu and Sudo, 1994; Sudo, 1986). Because the subduction supplies oxygen to the deeper layers of JSPW, the modern Japan Sea is oxic down to its bottom (Gamo *et al.*, 1986).

Sediment core

The sediment core IWANAI No. 3 was collected offshore of Iwanai, Hokkaido (43°22′36″ N, 140°04′10″ E, water depth 900 m) in November 1998 during a cruise of the Koyo-Maru that was operated by the Nippon Salvage Co. Ltd. The sampling point and the lithology of the

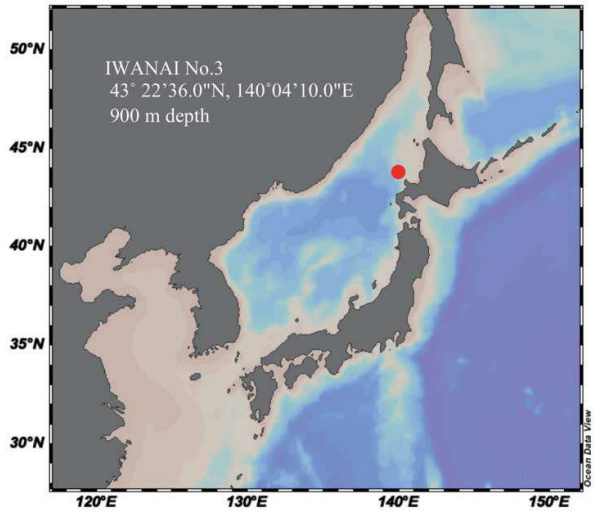

Fig. 1. Location of the sampling point of the IWANAI No. 3 core.

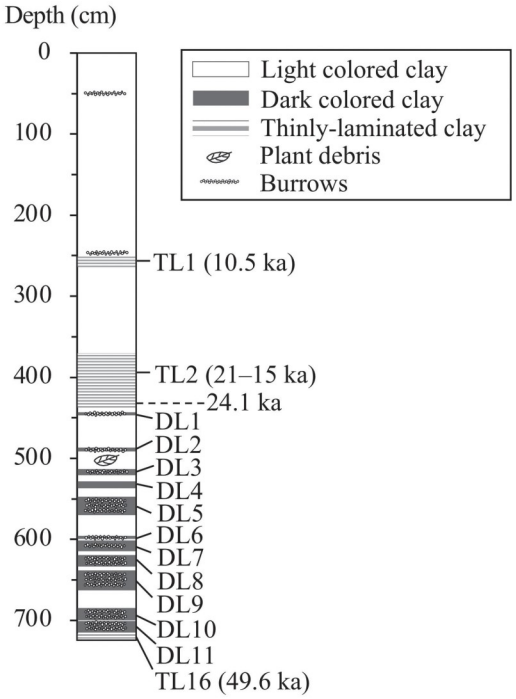

Fig. 2. Lithology of the IWANAI No. 3 core. The dark layers are numbered sequentially from the top of the core. The upper two and bottom laminated clay layers correspond to TL1, TL2, and TL16 in the literature.

IWANAI No. 3 core are shown in Figs. 1 and 2, respectively. The IWANAI No. 3 core consists of light colored clay, dark colored clay, and thinly-laminated clay as previously observed for cores in the literature (Ikehara and Itaki, 2007; Nakajima *et al.*, 1996; Oba *et al.*, 1991). Dark colored clay layers (DL) are numbered sequentially from the top of the core. The upper two and bottom thinly-laminated clay layers (TL) correspond to TL1, TL2, and TL16 in the literature (Oba *et al.*, 1991; Tada *et al.*, 1999). Burrows of slight bioturbation are observed in a layer at a 50 cm depth from the top, and burrows of moderate bioturbation are observed in layers at 242 cm and 370 cm depths and in all DLs. In addition, all DLs are rich in foraminifera. TL1 is rich in foraminifera but bioturbation is absent. Radiocarbon dating indicates that the bottom of TL2 (428 cm) and the bottom of TL16 (725 cm) were deposited at 20.53 ± 0.12 ka [24,266 to 23,930 cal BP (1σ)] and 46.5 ± 0.4 ka [(49,970 to 49,157 cal BP (1σ)] as ^{14}C ages, respectively. Monospecies planktonic foraminifera (*Globigerina bulloides*) were handpicked, and dated by accelerator mass spectrometry at the Christian-Albrechts University, Kiel, Germany. The ^{14}C ages were calibrated to calendar ages using OxCal (Bronk Ramsey, 2009). The local effect of the marine reservoir (ΔR) was set at +95 ± 60 yr, in the northern Japan Sea (Kuzmin *et al.*, 2007).

Based on a stratigraphic comparison with other sediment cores from the Japan Sea, we estimated that TL1 (254–257 cm) was deposited at 10.5 ka and TL2 (373–428 cm) was deposited during the Last Glacial Maximum (LGM) (15–21 ka) (Ikehara, 2003; Oba *et al.*, 1995). The deposition ages of the other layers were estimated by interpolation.

Ninety-nine subsamples were collected from different layers of the IWANAI No. 3 core using a Neoflon spoon. The subsamples were stored in polyethylene bags (Unipack E-4, Seisannipponsha, Japan), dried at 80°C for 24 h, crushed using a mallet, and kept in a desiccator.

Measurement of C, N, and S

Concentrations of total carbon (C_{tot}), organic carbon (C_{org}), total nitrogen (N_{tot}), and total sulfur (S_{tot}) in bulk sediment samples were determined using a FlashEA 1112 Analyzer (Thermo Fisher Scientific, USA) at the Center for Advanced Marine Core Research, Kochi University. For the measurement of C_{tot}, N_{tot}, and S_{tot}, a dried sediment sample (~5 mg) was directly introduced to the instrument and analyzed. For the measurement of C_{org}, a dried sediment sample (~0.5 g) was added with 50 mL of 1.3 mol kg^{-1} HCl and heated at 80°C for 12 h to remove carbonates. Then, the acid-treated residues were rinsed with distilled water and dried. A portion of this sample (~0.5 mg) was used to determine C_{org}. The concentration of inorganic carbon (C_{inorg}) was obtained by subtracting C_{org} from C_{tot}. In measurements of C, N, and S, the error of analyses was less than 2% as the relative standard deviation (RSD) for a standard material (C: 42%, N: 16%, and S: 19%). The C_{org} values were significantly higher

than C_{tot} in several samples. The abnormal C_{org} values were removed from discussion because the contamination of C was suspected during the acid treatment.

Measurement of metal concentrations

We used a microwave decomposition system (Speed Wave MWS-3$^+$, Analytik Jena) for digestion of sediments. A dried sediment sample (~100 mg) was weighed and placed in a digestion vessel named DAP 100. Two mL of H_2O_2 (30 wt%), 4 mL HNO_3 (60 wt%), 6 mL HCl (36 wt%), and 1 mL HF (46 wt%) were added to the digestion vessel, and the mixture was heated stepwise to 180°C for 1 h. The solution was evaporated to dryness and the solid residues were re-dissolved with 40 mL of 1 mol kg^{-1} HNO_3. Concentrations of major elements (Al, P, Ca, Ti, Mn, Fe, and Ba) were determined using an ICP-AES Optima 2000DV (Perkin Elmer, USA) after diluting the sample solution 25 times with 1 mol kg^{-1} HNO_3. Trace elements (V, Cr, Ni, Co, Cu, and Zn) in the undiluted sample solution were determined by ICP-AES. Other trace metals (Mo, Cd, Sb, W, and U) were determined using a Q-ICP-MS ELAN DRC II (Perkin Elmer) after diluting the sample solution 10 times. The Optima 2000DV and ELAN DRC II were equipment at the Institute for Chemical Research, Kyoto University. RSD for analysis of the standard material of sediments (NSC DC 74301) was below 1% for major elements and below 3% for trace elements, respectively.

Measurement of the isotope ratios of Mo and W

The analytical method reported in Tsujisaka *et al.* (2019) was used for the measurement of the isotope ratios of Mo and W. An aliquot of a sample (~100 mg) was decomposed using a microwave decomposition system (Speed Wave MWS-3$^+$). Then, we used two types of columns loaded with NOBIAS Chelate PA-1 resin (Hitachi High-Technologies, Japan) or AG1-X8 anion exchange resin (Bio Rad, USA) to separate Mo and W from each other and from matrix elements in the marine sediments. The resulting solutions were 0.15 mol kg^{-1} HNO_3 for Mo and 5.5 mmol kg^{-1} tetramethylammonium hydroxide (TMAH) for W. The isotopic composition and concentration of Mo or W in each solution were measured using a Neptune Plus MC-ICP-MS (Thermo Fisher Scientific, USA) at the Research Institute for Human and Nature (RIHN). The instrumental mass bias was corrected by standard-sample bracketing, combined with external correction using Ru for Mo and Re for W. The isotope ratios of Mo and W are presented as the delta value of δ^{98}Mo relative to the NIST SRM 3134 standard (Goldberg *et al.*, 2013; Greber *et al.*, 2012; Nägler *et al.*, 2014) and δ^{186}W (‰) relative to the NIST SRM 3163 standard (Irisawa and Hirata, 2006), respectively:

$$\delta^{98}\mathrm{Mo} = \left(\frac{\left({}^{98}\mathrm{Mo}/{}^{95}\mathrm{Mo}\right)_{\mathrm{sample}}}{\left({}^{98}\mathrm{Mo}/{}^{95}\mathrm{Mo}\right)_{\mathrm{NIST\ SRM\ 3134}}} - 1 \right) \times 1000 + 0.25 \quad (1)$$

$$\delta^{186}\mathrm{W} = \left(\frac{\left({}^{186}\mathrm{W}/{}^{184}\mathrm{W}\right)_{\mathrm{sample}}}{\left({}^{186}\mathrm{W}/{}^{184}\mathrm{W}\right)_{\mathrm{NIST\ SRM\ 3163}}} - 1 \right) \times 1000. \quad (2)$$

δ^{98}Mo of the NIST SRM 3134 standard is defined as +0.25‰, in accordance with Nägler *et al.* (2014), for a convenient comparison with the literature. The external reproducibility in the 95% confidence interval was 0.02–0.08‰ for δ^{98}Mo and 0.02–0.09‰ for δ^{186}W for standard materials of sediments (NSC DC 74301, JMS-1, JMS-2, CRM 7302-a, and HISS-1) (Tsujisaka *et al.*, 2019).

Results and Discussion

Depth profiles of elements

The C_{tot} concentration varied from 0.64% to 3.82%, the C_{org} concentration varied from 0.17% to 2.74%, and the C_{inorg} concentration varied from 0% to 2.40% (Supplementary Fig. S1). C_{tot} showed peaks at TL1, just above and top of TL2, and at DLs below 530 cm. The depth profile of C_{org} was mostly similar to that of C_{tot} but showed no peak at the top of TL2. C_{org} was strongly correlated with N_{tot} (r = 0.91) (Supplementary Table S2). These results can be ascribed to enhanced primary productivity in surface waters when these layers were formed. In contrast, substantial peaks of C_{inorg} and Ca occurred only at TL1, just above TL2, at the top of TL2, and at DL11. These peaks imply an enhanced deposition of carbonates in the period when these layers were formed.

The concentration of Al varied from 5.32% to 8.60% (Fig. S1). A significant decrease in Al appeared at TL1, just above TL2, and at TL16, implying the dilution of aluminosilicate minerals with carbonates. Aluminum showed strong correlations with Ti (r = 0.95), Co (r = 0.83), and W (r = 0.87) (Table S2).

The concentration of S_{tot} varied from 0.21% to 2.45% and showed sharp peaks at TL1, just above TL2, at the top of TL2, at DL5, and at DL11 (Fig. S1). S_{tot} shows the highest correlation with Ca (r = 0.50) and Mo (r = 0.50) (Table S2). The concentration of Mo varied from 1.0 ppm to 29.4 ppm, and peaks at TL1, TL2, DL5, and DL11 occurred concurrently with S_{tot}. These results suggested the formation of thiomolybdate caused by the occurrence of H_2S in bottom water and/or in pore water of the sediments (Helz *et al.*, 1996, 2004). The duration time of the sulfidic conditions was less than 500 y at DL5 and DL11, whereas it lasted 1100 y at TL1 and 3100 y at TL2. The Fe/Al (g/g) ratio also peaked together with S_{tot} and Mo (Supple-

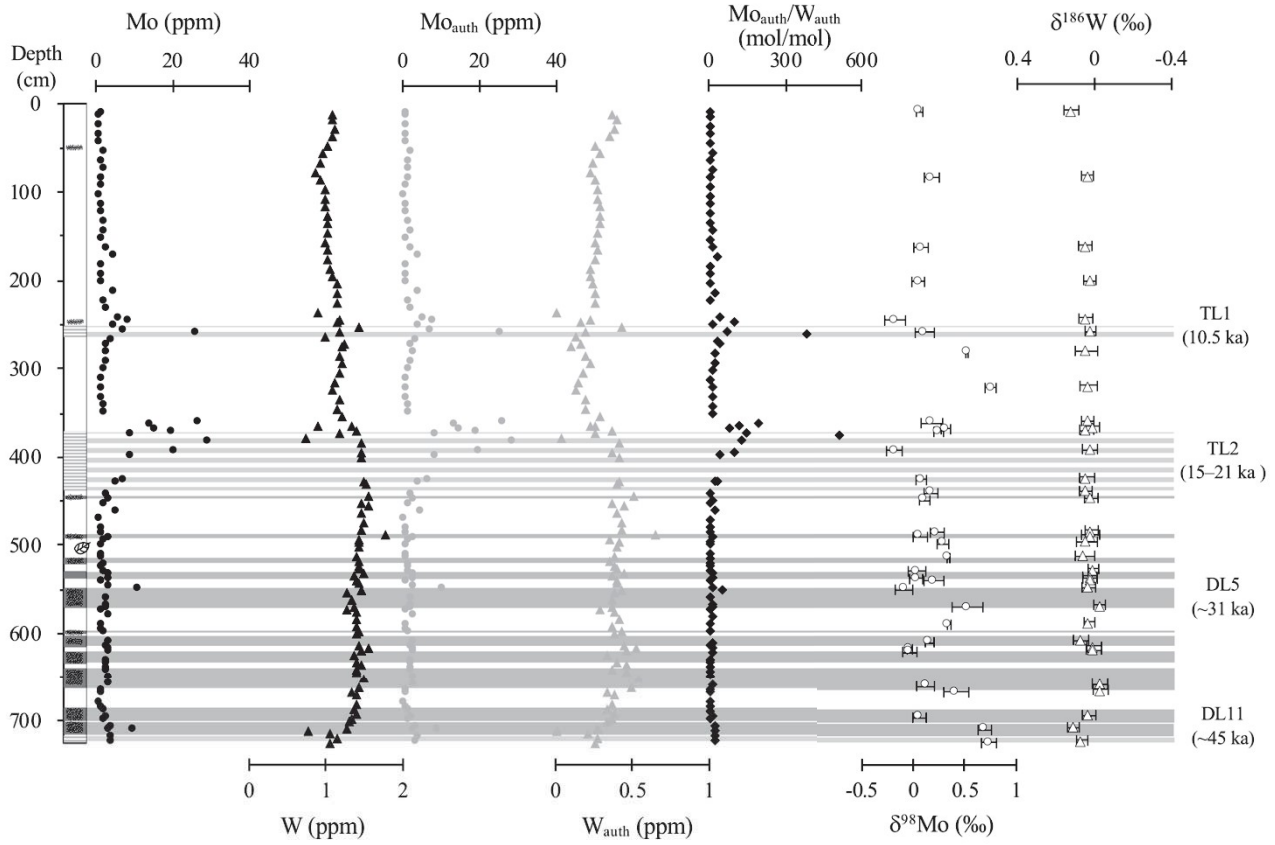

Fig. 3. Depth profiles of Mo, W, Mo_{auth}, and W_{auth} concentrations, the Mo_{auth}/W_{auth} (mol/mol) ratio, and isotopic compositions of Mo and W in the IWANAI No. 3 core. For δ^{98}Mo and δ^{186}W, the error bars show twice the internal standard error (±2SE) during each measurement. The light gray stripes and the dark gray bars indicate TLs and DLs, respectively. The black, gray, and white circles are data of Mo, Mo_{auth}, and δ^{98}Mo, respectively. The black, gray, and white triangles are data of W, W_{auth}, and δ^{186}W, respectively. The black diamonds are data of Mo_{auth}/W_{auth}.

mentary Fig. S3), thereby suggesting the deposition of iron sulfide. The peaks of the Mn/Al ratio occurred just above TL2, at the top of TL2, and at DL11 concurrently with those of C_{inorg} and Ca (Fig. S3), suggesting the deposition of manganese carbonate. The concentration of V varied from 57 ppm to 163 ppm and peaked at TL1 and several DLs (Supplementary Fig. S2). The concentration of U varied from 2.0 ppm to 14.7 ppm and peaked at TL1 and TL16 (Fig. S2). Previous studies have reported that V and U are redox-sensitive and removed from anoxic seawater in the absence of H_2S (Klinkhammer and Palmer, 1991; Morford and Emerson, 1999; Tribovillard *et al.*, 2006; Wanty and Goldhaber, 1992). The correlation between V and U was high ($r = 0.61$), although the correlations between V and Mo ($r = 0.19$) and between U and Mo ($r = 0.35$) were low (Table S2).

The depth profile of W was fairly uniform and in a range of 0.71–1.75 ppm. The baseline value of the W/Al profile was ~1.7×10^{-5} between 10 ka and the present (Fig. S3), which was significantly higher than the W/Al ratio of 1.2×10^{-5} in the crust (Rudnick and Gao, 2003); this suggested the authigenic removal of W from seawater by adsorption on Mn and Fe (oxyhydr)oxides. The W/Al ratio decreased at a 2.30 m depth, at the top of TL2, and in DL11 (Fig. S3). The decreases at TL2 and at DL11 were likely caused by the disappearance of Mn and Fe (oxyhydr)oxides in the euxinic sediments. An increase in W concentration in sulfidic waters has been observed in estuarine environments (Mohajerin *et al.*, 2016).

Quantitative analysis of variations in Mo and W concentrations

In this study, we assume that the concentration of an element in sediments (M_{sed}, ppm) is the sum of its contribution from lithogenic origin (M_{lith}) and authigenic origin (M_{auth}) sources (Siebert *et al.*, 2006):

$$M_{sed} = M_{lith} + M_{auth}. \quad (3)$$

M_{lith} and M_{auth} can be estimated by the following equations:

$$M_{lith} = Al_{sed} \times (M/Al)_{crust} \quad (4)$$

$$M_{auth} = M_{sed} - Al_{sed} \times (M/Al)_{crust} \quad (5)$$

where Al_{sed} (ppm) is the measured concentration of Al in the sediments and $(M/Al)_{crust}$ (g/g) is the ratio of the elemental M and Al in the crust. The ratio is 9.5×10^{-6} for Mo/Al and 1.2×10^{-5} for W/Al (Rudnick and Gao, 2003). The vertical profiles of Mo_{auth} and W_{auth} are presented in Fig. 3. The Mo_{auth}, W_{auth}, and M/Al ratios are listed in Supplementary Table S3. A previous study reported that the deep water of the Japan Sea became oxic by the formation of JSPW since 10 ka (Oba *et al.*, 1991). The results in the previous section also support the notion that the sediments of the IWANAI No. 3 core were deposited under oxic conditions since 10 ka. Mo_{auth} and W_{auth} showed a constant baseline value during this period; Mo_{auth} was 1.47 ± 0.92 ppm and W_{auth} was 0.27 ± 0.07 ppm. Although the baseline value of Mo_{auth} is almost constant throughout the core, Mo_{auth} increases up to 28.6 ppm at TL1, TL2, DL5, and DL11 (Fig. 3). In contrast, W_{auth} varied in a small range (0–0.64 ppm). Positive peaks of W_{auth} occurred just above TL1 and at DL2. Negative peaks of W_{auth} occurred at a 230 cm depth, at the top of TL2, and in DL11. In addition, the average values for W_{auth} shifted from 0.38 ± 0.09 ppm to the contemporary value of 0.24 ± 0.08 ppm after the LGM just above TL2 (Fig. 3).

Under oxic conditions, a major sink of Mo and W is the adsorption on Mn and Fe (oxyhydr)oxides (Barling *et al.*, 2001; Goldberg *et al.*, 2009; Kashiwabara *et al.*, 2013; Shimmield and Price, 1986). Assuming the system is at equilibrium, the adsorption of a metal on Mn and Fe (oxyhydr)oxides from seawater can be evaluated by the distribution coefficient (D):

$$D(M) = [M]_{ox}/[M]_{sw}, \quad (6)$$

where $[M]_{ox}$ (mol kg^{-1}) is the concentration of a metal adsorbed on Mn and Fe (oxyhydr)oxides and $[M]_{sw}$ (mol kg^{-1}) is the concentration of the metal in seawater; $[Mo]_{sw}$ = 107 nmol kg^{-1} and $[W]_{sw}$ = 49 pmol kg^{-1} (Firdaus *et al.*, 2008; Nakagawa *et al.*, 2012; Sohrin *et al.*, 1987). The literature indicates that D(W) is substantially higher than D(Mo). D(Mo) is 5.0×10^4 and D(W) is 3.5×10^6 for δ-MnO_2 in laboratory experiments (Sohrin *et al.*, 1999), D(Mo) is 2.8×10^3 and D(W) is 1.8×10^5 for $Fe(OH)_3$ in laboratory experiments (Ishibashi *et al.*, 1960; Sohrin *et al.*, 1987), and D(Mo) is 5.0×10^4 and D(W) is 1.1×10^7 for ferromanganese crusts on seamounts (Takematsu *et al.*, 1990). Using Eq. (6), the $[Mo]_{ox}/[W]_{ox}$ (mol/mol) ratio was calculated as 31 for δ-MnO_2, 34 for $Fe(OH)_3$, and 10 for ferromanganese crusts. The depth profile of Mo_{auth}/W_{auth} (mol/mol) is shown in Fig. 3 and Table S3. The baseline of Mo_{auth}/W_{auth} was 10.5 ± 7.3, which is in the range of the $[Mo]_{ox}/[W]_{ox}$ ratios calculated above, thereby supporting the control of Mn and Fe (oxyhydr)oxides on Mo_{auth} and W_{auth} under oxic conditions.

At TL1, TL2, and DL5, the Mo_{auth}/W_{auth} ratio greatly exceeded $[Mo]_{ox}/[W]_{ox}$. S_{tot} showed a similar vertical profile as compared to the Mo_{auth}/W_{auth} ratio (Fig. 3); the background value of S_{tot} was 0.46 ± 0.16% and its peak values reached 2.5%. We define excess-S_{tot} as S_{tot} minus the baseline S_{tot}. At TL1, TL2, DL5, and DL11, the Mo_{auth}/excess-S_{tot} (mol/mol) ratio ranged from 5.5×10^{-3} to 3.0×10^{-2} (Table S3). In a euxinic solution, Mo reacts with H_2S to form a reactive thiomolybdate anion, which is effectively removed from the solution (Emerson and Huested, 1991; Helz *et al.*, 1996, 2004). According to a study in the Black Sea water column (Erickson and Helz, 2000), the action point of switch (APS) occurred at a H_2S concentration of ~11 μmol kg^{-1}. In a study of pore water in the Santa Barbara Basin sediments, the first critical concentration of H_2S was ~0.1 μmol kg^{-1}, at which authigenic Mo formation likely occurred because of coprecipitation as a Mo-S-Fe phase (Zheng *et al.*, 2000). In contrast, W requires a much higher H_2S concentration (~60 μmol kg^{-1}) for the formation of thiotungstate, which is highly soluble in a sulfidic solution (Mohajerin *et al.*, 2016). Thus, Mo is preferentially removed from a weakly euxinic solution, resulting in the high Mo_{auth}/W_{auth} ratio observed in the current study. In previous studies, only the Mo concentration was investigated. In this study, by using the Mo/W ratio, we quantitatively detected the succession of hosts of Mo and W from Mn and Fe (oxyhydr)oxides to sulfides.

Behavior of δ^{98}Mo and δ^{186}W

The vertical profile of δ^{98}Mo in the sediment core ($\delta^{98}Mo_{sed}$) is shown in Fig. 3. $\delta^{98}Mo_{sed}$ varied from –0.19‰ to 0.75‰ and did not correlate with the concentration of Mo_{sed} (r = 0.21, Table S2). We argue that there are two important findings from these patterns. First, the peaks of $\delta^{98}Mo_{sed}$ did not correspond to those of Mo_{auth} (at TL1, TL2, DL5, and DL11, Fig. 3). In addition, $\delta^{98}Mo_{sed}$ did not show strong correlations with any parameters (Table S2). When the H_2S concentration in the bottom water exceeds 11 μmol kg^{-1}, Mo is completely removed from seawater and accumulates in sediments, and $\delta^{98}Mo_{sed}$ approaches the isotopic value of seawater $\delta^{98}Mo_{sw}$ = 2.34‰ (Nägler *et al.*, 2014). It is thus unlikely that the bottom water at this site experienced such a high H_2S concentration since 47 ka. Second, although $\delta^{98}Mo_{sed}$ was at an almost constant value of 0.09 ± 0.06‰ since 10

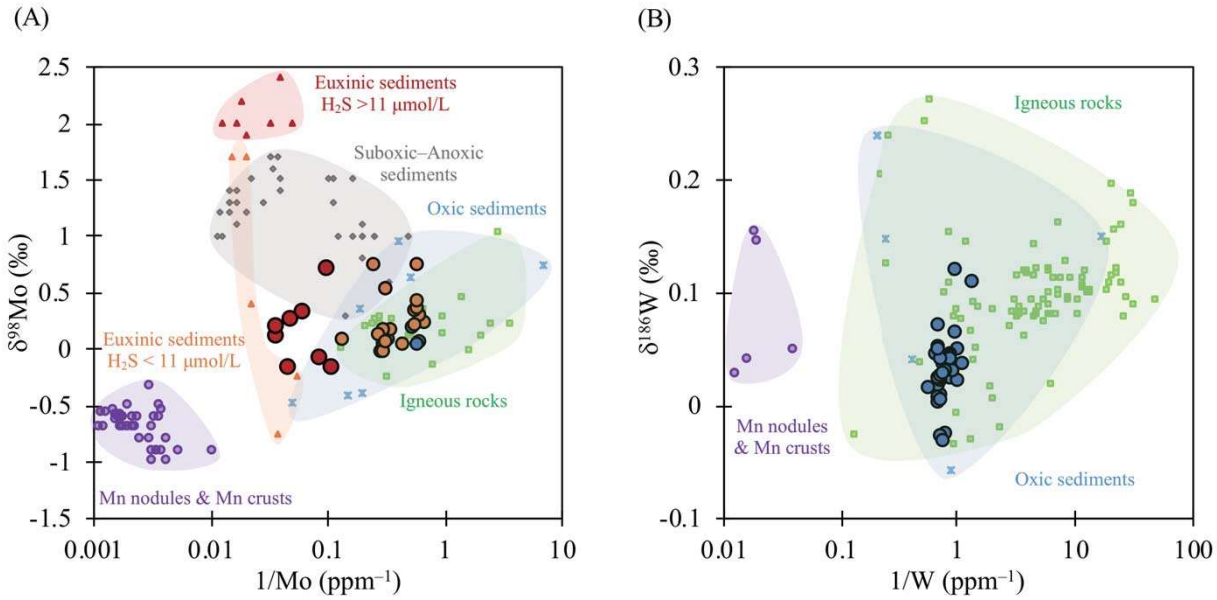

Fig. 4. A) Plots of δ^{98}Mo against the reciprocal of Mo concentration. The blue circles indicate the data of the IWANAI No. 3 core since 10 ka, the orange circles indicate the data during the period between 47 and 10 ka, and the red circles indicate the data at TL1, TL2, DL5, and DL11. The red and orange triangles are data of the Black Sea sediments with H_2S > 11 μmol kg^{-1} and H_2S < 11 μmol kg^{-1}, respectively. The gray diamonds are data of suboxic-anoxic sediments with O_2 < 10 μmol kg^{-1} and without H_2S. Blue crosses, green squares, and purple circles are data of oxic sediments, igneous rocks, and manganese nodules and manganese crusts, respectively. B) The plots of δ^{186}W against the reciprocal of W concentration. Blue circles indicate the data in the IWANAI No. 3 core. Blue crosses, green squares, and purple circles indicate data of oxic sediments, igneous rocks, and manganese nodules and manganese crusts, respectively.

ka, $\delta^{98}Mo_{sed}$ varied from –0.19‰ to 0.75‰ during 47–10 ka.

Molybdenum deposited in sediments under oxic conditions is a mixture of Mo in lithogenic debris and Mo from seawater adsorbed on Mn and Fe (oxyhydr)oxides. δ^{98}Mo in crustal rocks ranges from –0.3‰ to 1.0‰ (Burkhardt *et al.*, 2014; Hin *et al.*, 2013; Li *et al.*, 2014; Tsujisaka *et al.*, 2019; Willbold *et al.*, 2016; Zhao *et al.*, 2016). Based on laboratory experiments, the adsorption of Mo from seawater onto Mn and Fe (oxyhydr)oxides under oxic conditions causes isotopic fractionation, resulting in a positive $\Delta^{98}Mo_{sw\text{-}ox} = \delta^{98}Mo_{sw} - \delta^{98}Mo_{ox}$; in previous studies, this value was 2.4–2.9‰ for the adsorption on manganese oxide and 1.0–1.3‰ for the adsorption on ferrihydrite (Barling and Anbar, 2004; Goldberg *et al.*, 2009; Kashiwabara *et al.*, 2011, 2017; Wasylenki *et al.*, 2011). The observed δ^{98}Mo in ferromanganese oxides ranges from –1.0‰ to –0.3‰ (Barling *et al.*, 2001; Goto *et al.*, 2015; Siebert *et al.*, 2003; Tsujisaka *et al.*, 2019; Zhao *et al.*, 2016), and δ^{98}Mo in oxic marine sediments ranges from –0.5‰ to 0.9‰ (Li *et al.*, 2014; Tsujisaka *et al.*, 2019; Zhao *et al.*, 2016). $\delta^{98}Mo_{sed}$ in the IWANAI No. 3 core since 10 ka is consistent with these data, further supporting the presence of oxic conditions during this period.

An isotopic offset between $\delta^{98}Mo_{sw}$ and $\delta^{98}Mo_{sed}$ has been reported in sediments of weakly restricted or intermittently euxinic basins. For example, $\delta^{98}Mo_{sed}$ was 0.4–0.6‰ in the Gotland Deep in the Baltic Sea (Nägler *et al.*, 2011). A similar $\delta^{98}Mo_{sed}$ was observed in sediments above a bottom depth of 500 m in the Black Sea (Nägler *et al.*, 2011). Two likely mechanisms for this offset have been reported in the literature (Scholz *et al.*, 2013). One mechanism refers to the incomplete scavenging of intermediate thiomolybdate species (i.e., MoO_3S^{2-}, $MoO_2S_2^{2-}$, and $MoOS_3^{2-}$) when the concentration of H_2S is less than 11 μmol kg^{-1} (Neubert *et al.*, 2008). These intermediate thiomolybdate species deflect $\delta^{98}Mo_{sed}$ towards a lighter isotopic value from $\delta^{98}Mo_{sw}$ (Kerl *et al.*, 2017). In addition, short seawater residence times limit the reaction between Mo and H_2S, resulting in the formation of intermediate thiomolybdate species and an increase in the isotopic offset between $\delta^{98}Mo_{sw}$ and $\delta^{98}Mo_{sed}$ (Dahl *et al.*, 2010). Another mechanism is based on a Mn and Fe "shuttle" for Mo (Scholz *et al.*, 2013). At the interface between anoxic and oxic waters in the water column, Mn and Fe (oxyhydr)oxides are actively formed and scavenge lighter Mo isotopes preferentially from seawater, which

Table 1. Ages and Mo concentration when Mo peaks are present in this study and literatures

Sediment core	KCEs-1	ROV07-2	PC9	IWANAI No. 3	1246	1239
Literature	Zou *et al.* (2012)	Xu *et al.* (2014)	Crusius *et al.* (1999)	This study	Khim *et al.* (2012)	Khim *et al.* (2012)
Latitude	35°56′09″ N	36°05′51″ N	39°34′19″ N	43°22′36″ N	43°46′00″ N	44°48′00″ N
Longitude	130°41′55″ E	130°06′19″ E	139°24′30″ E	140°04′10″ E	138°50′00″ E	139°42′00″ E
Depth	1464 m	1500 m	807 m	900 m	3435 m	840 m
Age (ka)						
5					260	
9	28	32				7
10	27	24		9		10
11	35	28	8	26		14
13	17	16				
15	11	11		27		24
16		25	55	29		8
17		8	80	21	60	40
18	40	17	45	9	80	22
19	—	8	55	—	70	35
20	29	12	20	7	80	20
21	30	27		5	80	14
30	47			11		9
45	55			10		

are then carried to the sediments. During early diageneses, Mn and Fe (oxyhydr)oxides are reduced and re-dissolved, but a portion of Mo is transformed into thiomolybdates and eventually buried in association with metal sulfides and/or organic matter. We could not determine the most probable offset mechanism based on this study's data. We also could not explain the detailed mechanism of the variations in $\delta^{98}Mo_{sed}$ between 47 and 10 ka, although they may suggest that the redox conditions substantially changed in the bottom water and/or in pore water.

Figure 4A shows the isotope ratio of Mo plotted against the reciprocal of the Mo concentration in the IWANAI No. 3 core in comparison with values from a wide variety of geological samples in the literature (Nägler *et al.*, 2005; Neubert *et al.*, 2008; Poulson-Brucker *et al.*, 2009; Scholz *et al.*, 2017; Siebert *et al.*, 2003, 2006; Tsujisaka *et al.*, 2019; Zhao *et al.*, 2016). The values in the last 10 ka in the IWANAI No. 3 core were in the range of the values for igneous rocks and oxic sediments. The values during the period between 47 and 10 ka in the IWANAI No. 3 core plotted within the intermediate area between igneous rocks and suboxic-anoxic sediments. The values of TL1, TL2, DL5, and DL11 shifted to the area of euxinic sediments under the bottom water, with $H_2S < 11$ μmol kg^{-1}. These results support the validity of our data.

The vertical profile of $\delta^{186}W_{sed}$ is shown in Fig. 3. $\delta^{186}W_{sed}$ was almost constant throughout the IWANAI No. 3 core (–0.03~0.12‰), suggesting that there was no substantial change in the nature of source and sink of W. $\delta^{186}W_{sed}$ in the IWANAI No. 3 core is in a range of $\delta^{186}W$ reported for geological materials (–0.05~0.25‰) (Irisawa and Hirata, 2006; Krabbe *et al.*, 2017; Kurzweil *et al.*, 2018, 2019; Tsujisaka *et al.*, 2019). Takahashi *et al.* (2007) and Bodeï *et al.* (2007) suggested that the Mn/Fe ratio in marine sediments can be a proxy to distinguish hydrogenetic, diagenetic, and hydrothermal origins. The Mn/Fe ratio in the IWANAI No. 3 core was fairly constant, ranging from $0.73 \times 10^{-2} - 1.97 \times 10^{-2}$ (Table S3); this was consistent with the results of W. Previous studies have reported that strong anoxic conditions developed during the period between 27 and 20 ka (Oba *et al.*, 1991, 1995). Although fractionation in $\delta^{186}W$ during the adsorption of tungstate on Mn and Fe (oxyhydr)oxides has been reported (Mohajerin *et al.*, 2016), a similar fractionation of thiotungstate has not been reported yet. Fractionation in $\delta^{186}W$ will likely change depending on the speciation of W. Our $\delta^{186}W_{sed}$ data do not suggest that a formation of thiotungstate occurred and that the H_2S concentration rose above 60 μmol kg^{-1}.

Although $\delta^{186}W_{sed}$ is constant, a significant negative shift in W concentration occurred at 14.5 ka. Similar shifts are also observed in metals with high crustal abundances, such as Al, Ti, and Fe (Rudnick and Gao, 2003). Furthermore, the W concentrations show high correlations with those of Al ($r = 0.87$), Ti ($r = 0.85$), Fe ($r = 0.71$), Co ($r = 0.71$), Ni ($r = 0.78$), Cu ($r = 0.77$), and Zn ($r = 0.87$) (Table S2). The concentration shifts without a change in $\delta^{186}W_{sed}$ may imply a change in supply from the lithogenic sources. Previous studies have reported that the Japan Sea received inflow of surface water from the Yellow Sea and the East China Sea as well as an inflow of fresh water from rivers around the Japan Sea until 15 ka (Oba *et al.*, 1991, 1995). TWC became a major inflow after 10 ka. We observed an increase in W_{sw} and a concurrent decrease in salinity in the Yellow Sea and the East China Sea

(Sohrin *et al.*, 1999). Thus, it is possible that the supply of W to the Japan Sea was substantial higher before 15 ka compared to the present. In addition, strong anoxic conditions were developed in the deep-water layers of the Japan Sea during the period between 30 and 15 ka (Oba *et al.*, 1991, 1995). Because W is removed only in oxic sediments, the sink function of the sediment for W may have been reduced in the Japan Sea during this period. These conditions may have caused a higher steady concentration of W_{sw} in the Japan Sea.

Figure 4B shows the isotope ratio of W plotted against the reciprocal of the W concentration in the IWANAI No. 3 core in comparison with literature values of a variety of geological samples (Krabbe *et al.*, 2017; Kurzweil *et al.*, 2018, 2019; Tsujisaka *et al.*, 2019). The observed range of natural $\delta^{186}W$ is minor compared to that of $\delta^{98}Mo$. The values of $\delta^{186}W$ for the IWANAI No. 3 core occurred completely within an area of igneous rocks and oxic sediments. Therefore, this result indicate that the concentration and isotope ratio of W are not sensitive to redox change from oxic to weakly euxinic (11 μmol kg^{-1}) condition.

Synthesis of Mo concentration data in Japan Sea sediments

There are several reports measuring the concentration of Mo_{sed} in sediment cores collected from the Japan Sea (Table 1). Crusius *et al.* (1999) investigated a sediment core at an intermediate depth of the eastern Japan Sea (KT-94 PC9; 807 m depth) and Khim *et al.* (2012) investigated a sediment core at an intermediate depth of the northern Japan Sea (GH-99 1239; water depth 840 m). Both authors reported Mo_{sed} peaks at TL1 (10.5 ka) and TL2 (LGM). Moreover, the GH-99 1239 core also had a Mo_{sed} peak at 30 ka. Khim *et al.* (2012) also investigated a sediment core in the deepest area of the northern Japan Sea (GH-99 1246; 3435 m). Although the GH-9 1246 core had Mo_{sed} peaks at 5 ka and LGM, there was no peak at TL1. The sediment cores in the Tsushima Basin were investigated by Xu *et al.* (2014) and Zou *et al.* (2012). Both cores of KCEs-1 (1464 m) and ROV07-2 (1500 m) showed concurrent peaks of Mo_{sed} since 11 ka. In contrast, Mo_{sed} showed larger variations before 11 ka, and the variations of Mo_{sed} were not concurrent between the two cores. The authors inferred that the bottom water became euxinic when Mo_{sed} was high. The Mo_{sed} concentration was less than 80 ppm, except for 260 ppm at 5 ka of GH-99 1246.

The Mo_{sed} peaks since 11 ka were concurrent among sediment cores collected at intermediate depths in the Japan Sea, whereas the peak concentrations differed depending on the sites (Table 1). This suggests that a concurrent variation in the redox condition occurred in the entire Japan Sea. Our hypothesis based on $\delta^{98}Mo_{sed}$ may therefore apply to the entire Japan Sea. The accumulation of Mo_{sed} may have occurred in euxinic bottom water with less than 11 μmol kg^{-1} H_2S or in pore water in sediments below the oxic-anoxic interface in the water column where simultaneously perform the Mn and Fe shuttle work. Therefore, we insist that measurements of Mo isotope compositions along with Mo concentrations are important for accurately estimating the redox conditions of the bottom environment. The literature suggests that the depth of the Japan Sea experienced alteration between anoxic and oxic conditions before 15 ka (Itaki *et al.*, 2004; Oba *et al.*, 1991, 1995; Tada *et al.*, 1999). Table 1 shows that the timing and magnitude of Mo peaks in the Japan Sea sediments deposited before 15 ka varied substantially depending on the site and water depth. Thus, it is likely that the redox conditions were highly heterogeneous in the deep-water layers of the Japan Sea during the last glacial age.

CONCLUSIONS

In this study, we report the concentrations and isotopic compositions of Mo and W in the IWANAI No. 3 core in the northern Japan Sea along with other elements, such as C, N, S, Al, Ca, V, Mn, Fe, and U. Based on an analysis of the Mo/W ratio, we estimate that H_2S appeared in the bottom and/or pore water at TLs and DLs of 11–10 ka, 17–14 ka (LGM), 31 ka, and 45 ka. The Mo/W ratio suggests that bottom water at the other TLs and DLs was oxic as well as when light colored clay was deposited. Because $\delta^{98}Mo_{sed}$ in the IWANAI No. 3 core was significantly lower than $\delta^{98}Mo_{sw}$, the H_2S concentration in seawater was estimated to be less than 11 μmol kg^{-1}. These results provide additional and semi-quantitative constraints on the redox conditions discussed in previous studies. A negative shift of the W_{auth} depth profile occurring at 15 ka suggested a regime shift in the Japan Sea, which is consistent with the literature. In contrast, $\delta^{186}W_{sed}$ was almost constant throughout the IWANAI No. 3 core, indicating an absence of a substantial change in the source (contributions of lithogenic and hydrothermal sources) and sink (contributions of oxic and euxinic sinks) for W. The data of Mo and W consistently suggest suboxic or weakly reducing conditions with H_2S concentration less than 11 μmol kg^{-1} in the bottom water. We can say that the synthetic analysis of Mo and W more strictly constrain the paleoceanographic conditions. Moderate offsets between $\delta^{98}Mo_{sw}$ and $\delta^{98}Mo_{sed}$ were observed in layers of 47–10 ka; these have not been fully explained yet and must be detailed in a future investigation.

Acknowledgments—We would like to thank Ki-Cheol Shin (RIHN) for technical advice regarding MC-ICP-MS measurements. We would like to extend our appreciation to graduate students Daisuke Terui, Yui Morishima, and Shouhei Ichiwaki, who carried out the preliminary experiments of this study. This study was supported by KAKENHI grants (20654049,

21350042, 26610182, and 15H01727) from the Japan Society for the Promotion of Science (JSPS), Research Grants for Environmental Isotope Study from the Research Institute for Humanity and Nature (grant numbers 2016-7, 2017-8, 2018-15, and 2019-4), and Mitsumasa Ito Memorial Research Grants (grant number H30-R7 and H31-R2) from the Research Institute for Oceanochemistry Foundation. We also thank Editage (www.editage.jp) for English language editing.

References

Barling, J. and Anbar, A. D. (2004) Molybdenum isotope fractionation during adsorption by manganese oxides. *Earth. Planet. Sci. Lett.* **217**, 315–329.

Barling, J., Arnold, G. L. and Anbar, A. D. (2001) Natural mass-dependent variations in the isotopic composition of molybdenum. *Earth. Planet. Sci. Lett.* **193**, 447–457.

Bauer, S., Conrad, S. and Ingri, J. (2018) Geochemistry of tungsten and molybdenum during freshwater transport and estuarine mixing. *J. Appl. Geochem.* **93**, 36–48.

Bodeï, S., Manceau, A., Geoffroy, N., Baronnet, A. and Buatier, M. (2007) Formation of todorokite from vernadite in Ni-rich hemipelagic sediments. *Geochim. Cosmochim. Acta* **71**, 5698–5716.

Bronk Ramsey, C. B. (2009) Bayesian analysis of radiocarbon dates. *Radiocarbon* **51**, 337–360.

Burkhardt, C., Hin, R. C., Kleine, T. and Bourdon, B. (2014) Evidence for Mo isotope fractionation in the solar nebula and during planetary differentiation. *Earth. Planet. Sci. Lett.* **391**, 201–211.

Calvert, S. and Pedersen, T. (1993) Geochemistry of recent oxic and anoxic marine sediments: Implications for the geological record. *Mar. Geol.* **113**, 67–88.

Crusius, J., Calvert, S., Pedersen, T. and Sage, D. (1996) Rhenium and molybdenum enrichments in sediments as indicators of oxic, suboxic and sulfidic conditions of deposition. *Earth. Planet. Sci. Lett.* **145**, 65–78.

Crusius, J., Pedersen, T. F., Calvert, S. E., Cowie, G. L. and Oba, T. (1999) A 36 kyr geochemical record from the Sea of Japan of organic matter flux variations and changes in intermediate water oxygen concentrations. *Paleoceanography* **14**, 248–259.

Dahl, T. W. and Wirth, S. B. (2017) Molybdenum isotope fractionation and speciation in a euxinic lake—Testing ways to discern isotope fractionation processes in a sulfidic setting. *Chem. Geol.* **460**, 84–92.

Dahl, T. W., Anbar, A. D., Gordon, G. W., Rosing, M. T., Frei, R. and Canfield, D. E. (2010) The behavior of molybdenum and its isotopes across the chemocline and in the sediments of sulfidic Lake Cadagno, Switzerland. *Geochim. Cosmochim. Acta* **74**, 144–163.

Dellwig, O., Wegwerth, A., Schnetger, B., Schulz, H. and Arz, H. W. (2019) Dissimilar behaviors of the geochemical twins W and Mo in hypoxic-euxinic marine basins. *Earth-Sci. Rev.* **193**, 1–23.

Emerson, S. R. and Huested, S. S. (1991) Ocean anoxia and the concentrations of molybdenum and vanadium in seawater. *Mar. Chem.* **34**, 177–196.

Erickson, B. E. and Helz, G. R. (2000) Molybdenum(VI) speciation in sulfidic waters: Stability and lability of thiomolybdates. *Geochim. Cosmochim. Acta* **64**, 1149–1158.

Firdaus, M. L., Norisuye, K., Nakagawa, Y., Nakatsuka, S. and Sohrin, Y. (2008) Dissolved and labile particulate Zr, Hf, Nb, Ta, Mo and W in the Western North Pacific Ocean. *J. Oceanogr.* **64**, 247–257.

Gamo, T., Nozaki, Y., Sakai, H., Nakai, T. and Tsubota, H. (1986) Spacial and temporal variations of water characteristics in the Japan Sea bottom layer. *J. Mar. Res.* **44**, 781–793.

Goldberg, T., Archer, C., Vance, D. and Poulton, S. W. (2009) Mo isotope fractionation during adsorption to Fe (oxyhydr)oxides. *Geochim. Cosmochim. Acta* **73**, 6502–6516.

Goldberg, T., Gordon, G., Izon, G., Archer, C., Pearce, C. R., McManus, J., Anbar, A. D. and Rehkämper, M. (2013) Resolution of inter-laboratory discrepancies in Mo isotope data: an intercalibration. *J. Anal. At. Spectrom.* **28**, 724–735.

Goto, K. T., Shimoda, G., Anbar, A. D., Gordon, G. W., Harigane, Y., Senda, R. and Suzuki, K. (2015) Molybdenum isotopes in hydrothermal manganese crust from the Ryukyu arc system: Implications for the source of molybdenum. *Mar. Geol.* **369**, 91–99.

Greber, N. D., Siebert, C., Nägler, T. F. and Pettke, T. (2012) $\delta^{98/95}$Mo values and molybdenum concentration data for NIST SRM 610, 612 and 3134: Towards a common protocol for reporting Mo data. *Geostand. Geoanal. Res.* **36**, 291–300.

Helz, G. R., Miller, C., Charnock, J., Mosselmans, J., Pattrick, R., Garner, C. and Vaughan, D. (1996) Mechanism of molybdenum removal from the sea and its concentration in black shales: EXAFS evidence. *Geochim. Cosmochim. Acta* **60**, 3631–3642.

Helz, G. R., Vorlicek, T. P. and Kahn, M. D. (2004) Molybdenum scavenging by iron monosulfide. *Environ. Sci. Technol.* **38**, 4263–4268.

Hin, R. C., Burkhardt, C., Schmidt, M. W., Bourdon, B. and Kleine, T. (2013) Experimental evidence for Mo isotope fractionation between metal and silicate liquids. *Earth. Planet. Sci. Lett.* **379**, 38–48.

Ikehara, K. (2003) Late Quaternary seasonal sea-ice history of the northeastern Japan Sea. *J. Oceanogr.* **59**, 585–593.

Ikehara, K. and Itaki, T. (2007) Millennial-scale fluctuations in seasonal sea-ice and deep-water formation in the Japan Sea during the late Quaternary. *Palaeogeogr. Palaeoclimatol. Palaeoecol.* **247**, 131–143.

Irisawa, K. and Hirata, T. (2006) Tungsten isotopic analysis on six geochemical reference materials using multiple collector-ICP-mass spectrometry coupled with a rhenium-external correction technique. *J. Anal. At. Spectrom.* **21**, 1387–1395.

Ishibashi, M., Fujinaga, T., Kuwamoto, T., Koyama, M. and Sugibayashi, S. (1960) Chemical studies of the ocean. XXCIX: Coprecipitation of tungsten with ferric hydroxide. *J. Chem. Soc. Jpn.* **81**, 392–395.

Itaki, T., Ito, M., Narita, H., Ahagon, N. and Sakai, H. (2003) Depth distribution of radiolarians from the Chukchi and Beaufort Seas, western Arctic. *Deep-Sea Res. Part I Oceanogr. Res. Pap.* **50**, 1507–1522.

Itaki, T., Ikehara, K., Motoyama, I. and Hasegawa, S. (2004) Abrupt ventilation changes in the Japan Sea over the last 30 ky: evidence from deep-dwelling radiolarians. *Palaeogeogr. Palaeoclimatol. Palaeoecol.* **208**, 263–278.

Kashiwabara, T., Takahashi, Y., Tanimizu, M. and Usui, A. (2011) Molecular-scale mechanisms of distribution and isotopic fractionation of molybdenum between seawater and ferromanganese oxides. *Geochim. Cosmochim. Acta* **75**, 5762–5784.

Kashiwabara, T., Takahashi, Y., Marcus, M. A., Uruga, T., Tanida, H., Terada, Y. and Usui, A. (2013) Tungsten species in natural ferromanganese oxides related to its different behavior from molybdenum in oxic ocean. *Geochim. Cosmochim. Acta* **106**, 364–378.

Kashiwabara, T., Kubo, S., Tanaka, M., Senda, R., Iizuka, T., Tanimizu, M. and Takahashi, Y. (2017) Stable isotope fractionation of tungsten during adsorption on Fe and Mn (oxyhydr)oxides. *Geochim. Cosmochim. Acta* **204**, 52–67.

Kendall, B., Gordon, G. W., Poulton, S. W. and Anbar, A. D. (2011) Molybdenum isotope constraints on the extent of late Paleoproterozoic ocean euxinia. *Earth. Planet. Sci. Lett.* **307**, 450–460.

Kerl, C. F., Lohmayer, R., Bura-Nakic, E., Vance, D. and Planer-Friedrich, B. (2017) Experimental confirmation of isotope fractionation in thiomolybdates using ion chromatographic separation and detection by multicollector ICPMS. *Anal Chem.* **89**, 3123–3129.

Khim, B.-K., Tada, R., Park, Y. H., Bahk, J. J., Kido, Y., Itaki, T. and Ikehara, K. (2009) Correlation of TL layers for the synchronous paleoceanographic events in the East Sea (Sea of Japan) during the Late Quaternary. *Geosci. J.* **13**, 113–120.

Khim, B.-K., Ikehara, K. and Irino, T. (2012) Orbital- and millennial-scale paleoceanographic changes in the northeastern Japan Basin, East Sea/Japan Sea during the late Quaternary. *J. Quat. Sci.* **27**, 328–335.

Kishida, K., Sohrin, Y., Okamura, K. and Ishibashi, J. (2004) Tungsten enriched in submarine hydrothermal fluids. *Earth. Planet. Sci. Lett.* **222**, 819–827.

Klinkhammer, G. P. and Palmer, M. R. (1991) Uranium in the oceans: Where it goes and why. *Geochim. Cosmochim. Acta* **55**, 1799–1806.

Krabbe, N., Kruijer, T. S. and Kleine, T. (2017) Tungsten stable isotope compositions of terrestrial samples and meteorites determined by double spike MC-ICPMS. *Chem. Geol.* **450**, 135–144.

Kurzweil, F., Wille, M., Gantert, N., Beukes, N. J. and Schoenberg, R. (2016) Manganese oxide shuttling in pre-GOE oceans—evidence from molybdenum and iron isotopes. *Earth. Planet. Sci. Lett.* **452**, 69–78.

Kurzweil, F., Münker, C., Tusch, J. and Schoenberg, R. (2018) Accurate stable tungsten isotope measurements of natural samples using a ^{180}W-^{183}W double-spike. *Chem. Geol.* **476**, 407–417.

Kurzweil, F., Münker, C., Grupp, M., Braukmüller, N., Fechtner, L., Christian, M., Hohl, S. V. and Schoenberg, R. (2019) The stable tungsten isotope composition of modern igneous reservoirs. *Geochim. Cosmochim. Acta* **251**, 176–191.

Kuzmin, Y., Burr, G., Gorbunov, S., Rakov, V. and Razjigaeva, N. (2007) A tale of two seas: reservoir age correction values (R, ΔR) for the Sakhalin Island (Sea of Japan and Okhotsk Sea). *Nucl. Instrum. Meth. B* **259**, 460–462.

Li, J., Liang, X.-R., Zhong, L.-F., Wang, X.-C., Ren, Z.-Y., Sun, S.-L., Zhang, Z.-F. and Xu, J.-F. (2014) Measurement of the isotopic composition of molybdenum in geological samples by MC-ICP-MS using a novel chromatographic extraction technique. *Geostand. Geoanal. Res.* **38**, 345–354.

Lim, D., Xu, Z., Choi, J., Kim, S., Kim, E., Kang, S. and Jung, H. (2011) Paleoceanographic changes in the Ulleung Basin, East (Japan) Sea, during the last 20,000 years: Evidence from variations in element composition of core sediments. *Prog. Oceanogr.* **88**, 101–115.

Menard, H. and Smith, S. M. (1966) Hypsometry of ocean basin provinces. *J. Geophys. Res.* **71**, 4305–4325.

Minoura, K., Akaki, K., Nemoto, N., Tsukawaki, S. and Nakamura, T. (2012) Origin of deep water in the Japan Sea over the last 145kyr. *Palaeogeogr. Palaeoclimatol. Palaeoecol.* **339–341**, 25–38.

Mohajerin, T. J., Helz, G. R., White, C. D. and Johannesson, K. H. (2014) Tungsten speciation in sulfidic waters: Determination of thiotungstate formation constants and modeling their distribution in natural waters. *Geochim. Cosmochim. Acta* **144**, 157–172.

Mohajerin, T. J., Helz, G. R. and Johannesson, K. H. (2016) Tungsten-molybdenum fractionation in estuarine environments. *Geochim. Cosmochim. Acta* **177**, 105–119.

Morford, J. L. and Emerson, S. (1999) The geochemistry of redox sensitive trace metals in sediments. *Geochim. Cosmochim. Acta* **63**, 1735–1750.

Nägler, T. F., Siebert, C., Lüschen, H. and Böttcher, M. E. (2005) Sedimentary Mo isotope record across the Holocene fresh-brackish water transition of the Black Sea. *Chem. Geol.* **219**, 283–295.

Nägler, T. F., Neubert, N., Böttcher, M. E., Dellwig, O. and Schnetger, B. (2011) Molybdenum isotope fractionation in pelagic euxinia: Evidence from the modern Black and Baltic Seas. *Chem. Geol.* **289**, 1–11.

Nägler, T. F., Anbar, A. D., Archer, C., Goldberg, T., Gordon, G. W., Greber, N. D., Siebert, C., Sohrin, Y. and Vance, D. (2014) Proposal for an international molybdenum isotope measurement standard and data representation. *Geostand. Geoanal. Res.* **38**, 149–151.

Nakagawa, Y., Takano, S., Firdaus, M. L., Norisuye, K., Hirata, T., Vance, D. and Sohrin, Y. (2012) The molybdenum isotopic composition of the modern ocean. *Geochem. J.* **46**, 131–141.

Nakajima, T., Yoshikawa, K., Ikehara, K., Katayama, H., Kikawa, E., Joshima, M. and Seto, K. (1996) Marine sediments and late Quaternary stratigraphy in the Southeastern part of the Japan Sea—Concerning the timing of dark layer deposition—. *J. Geol. Soc. Japan* **102**, 125–138.

Neubert, N., Nägler, T. F. and Böttcher, M. E. (2008) Sulfidity controls molybdenum isotope fractionation into euxinic sediments: Evidence from the modern Black Sea. *Geology* **36**, 775–778.

Oba, T., Kato, M., Kitazato, H., Koizumi, I., Omura, A., Sakai, T. and Takayama, T. (1991) Paleoenvironmental changes in the Japan Sea during the last 85,000 years.

Paleoceanography **6**, 499–518.
Oba, T., Murayama, M., Matsumoto, E. and Nakamura, T. (1995) AMS-^{14}C ages of Japan Sea cores from the Oki Ridge. *Quat. Res. (Daiyonki-kenkyu)* **34**, 289–296.
Ostrander, C. M., Sahoo, S. K., Kendall, B., Jiang, G., Planavsky, N. J., Lyons, T. W., Nielsen, S. G., Owens, J. D., Gordon, G. W., Romaniello, S. J. and Anbar, A. D. (2019) Multiple negative molybdenum isotope excursions in the Doushantuo Formation (South China) fingerprint complex redox-related processes in the Ediacaran Nanhua Basin. *Geochim. Cosmochim. Acta* **261**, 191–209.
Poulson-Brucker, R. L., McManus, J., Severmann, S. and Berelson, W. M. (2009) Molybdenum behavior during early diagenesis: Insights from Mo isotopes. *Geochem., Geophys., Geosyst.* **10**.
Rudnick, R. L. and Gao, S. (2003) Composition of the continental crust. *Treatise Geochem.* **3**, 659.
Scholz, F., McManus, J. and Sommer, S. (2013) The manganese and iron shuttle in a modern euxinic basin and implications for molybdenum cycling at euxinic ocean margins. *Chem. Geol.* **355**, 56–68.
Scholz, F., Siebert, C., Dale, A. W. and Frank, M. (2017) Intense molybdenum accumulation in sediments underneath a nitrogenous water column and implications for the reconstruction of paleo-redox conditions based on molybdenum isotopes. *Geochim. Cosmochim. Acta* **213**, 400–417.
Scott, C. and Lyons, T. W. (2012) Contrasting molybdenum cycling and isotopic properties in euxinic versus non-euxinic sediments and sedimentary rocks: Refining the paleoproxies. *Chem. Geol.* **324–325**, 19–27.
Senjyu, T. and Sudo, H. (1994) The upper portion of the Japan Sea Proper Water; its source and circulation as deduced from isopycnal analysis. *J. Oceanogr.* **50**, 663–690.
Shimmield, G. and Price, N. (1986) The behaviour of molybdenum and manganese during early sediment diagenesis-offshore Baja California, Mexico. *Mar. Chem.* **19**, 261–280.
Siebert, C., Nägler, T. F., von Blanckenburg, F. and Kramers, J. D. (2003) Molybdenum isotope records as a potential new proxy for paleoceanography. *Earth. Planet. Sci. Lett.* **211**, 159–171.
Siebert, C., McManus, J., Bice, A., Poulson, R. and Berelson, W. M. (2006) Molybdenum isotope signatures in continental margin marine sediments. *Earth. Planet. Sci. Lett.* **241**, 723–733.
Sohrin, Y., Isshiki, K., Kuwamoto, T. and Nakayama, E. (1987) Tungsten in North Pacific waters. *Mar. Chem.* **22**, 95–103.
Sohrin, Y., Matsui, M. and Nakayama, E. (1999) Contrasting behavior of tungsten and molybdenum in the Okinawa Trough, the East China Sea and the Yellow Sea. *Geochim. Cosmochim. Acta* **63**, 3457–3466.
Sudo, H. (1986) A note on the Japan Sea proper water. *Prog. Oceanogr.* **17**, 313–336.
Tada, R. (1995) Possible Dansgaard-Oeschger oscillation signal recorded in the Japan Sea sediments. *Proc. of 1994 IGBP Symposium: Global Flux of Carbon and Its Related Substances in the Coastal Sea-Ocean-Atmosphere System.*
Tada, R., Irino, T. and Koizumi, I. (1999) Land-ocean linkages over orbital and millennial timescales recorded in late Quaternary sediments of the Japan Sea. *Paleoceanography* **14**, 236–247.
Takahashi, Y., Manceau, A., Geoffroy, N., Marcus, M. A. and Usui, A. (2007) Chemical and structural control of the partitioning of Co, Ce, and Pb in marine ferromanganese oxides. *Geochim. Cosmochim. Acta* **71**, 984–1008.
Takematsu, N., Sato, Y., Okabe, S. and Usui, A. (1990) Uptake of selenium and other oxyanionic elements in marine ferromanganese concretions of different origins. *Mar. Chem.* **31**, 271–283.
Thoby, M., Konhauser, K. O., Fralick, P. W., Altermann, W., Visscher, P. T. and Lalonde, S. V. (2019) Global importance of oxic molybdenum sinks prior to 2.6 Ga revealed by the Mo isotope composition of Precambrian carbonates. *Geology* **47**, 559–562.
Toba, Y. (1982) Seasonal and year-to-year variability of the Tsushima-Tsugaru Warm Current System with its possible cause. *La mer* **20**, 41–51.
Tribovillard, N., Algeo, T. J., Lyons, T. and Riboulleau, A. (2006) Trace metals as paleoredox and paleoproductivity proxies: An update. *Chem. Geol.* **232**, 12–32.
Tsujisaka, M., Takano, S., Murayama, M. and Sohrin, Y. (2019) Precise analysis of the concentrations and isotopic compositions of molybdenum and tungsten in geochemical reference materials. *Anal. Chim. Acta* **1091**, 146–159.
Wanty, R. B. and Goldhaber, M. B. (1992) Thermodynamics and kinetics of reactions involving vanadium in natural systems: Accumulation of vanadium in sedimentary rocks. *Geochim. Cosmochim. Acta* **56**, 1471–1483.
Wasylenki, L. E., Weeks, C. L., Bargar, J. R., Spiro, T. G., Hein, J. R. and Anbar, A. D. (2011) The molecular mechanism of Mo isotope fractionation during adsorption to birnessite. *Geochim. Cosmochim. Acta* **75**, 5019–5031.
Watanabe, S., Tada, R., Ikehara, K., Fujine, K. and Kido, Y. (2007) Sediment fabrics, oxygenation history, and circulation modes of Japan Sea during the Late Quaternary. *Palaeogeogr. Palaeoclimatol. Palaeoecol.* **247**, 50–64.
Watanabe, Y., Kashiwabara, T., Ishibashi, J., Sekizawa, O., Nitta, K., Uruga, T. and Takahashi, Y. (2017) Different partitioning behaviors of molybdenum and tungsten in a sediment-water system under various redox conditions. *Chem. Geol.* **471**, 38–51.
Willbold, M., Hibbert, K., Lai, Y. J., Freymuth, H., Hin, R. C., Coath, C., Vils, F. and Elliott, T. (2016) High-precision mass-dependent molybdenum isotope variations in magmatic rocks determined by double-spike MC-ICP-MS. *Geostand. Geoanal. Res.* **40**, 389–403.
Wille, M., Nagler, T. F., Lehmann, B., Schroder, S. and Kramers, J. D. (2008) Hydrogen sulphide release to surface waters at the Precambrian/Cambrian boundary. *Nature* **453**, 767–769.
Xu, Z., Lim, D., Choi, J., Li, T., Wan, S. and Rho, K. (2014) Sediment provenance and paleoenvironmental change in the Ulleung Basin of the East (Japan) Sea during the last 21 kyr. *J. Asian Earth. Sci.* **93**, 146–157.
Zhao, P. P., Li, J., Zhang, L., Wang, Z. B., Kong, D. X., Ma, J. L., Wei, G. J. and Xu, J. F. (2016) Molybdenum mass fractions and isotopic compositions of international geological reference materials. *Geostand. Geoanal. Res.* **40**, 217–226.
Zheng, Y., Anderson, R. F., Van Geen, A. and Kuwabara, J. (2000) Authigenic molybdenum formation in marine

sediments: a link to pore water sulfide in the Santa Barbara Basin. *Geochim. Cosmochim. Acta* **64**, 4165–4178.
Zou, J., Shi, X., Liu, Y., Liu, J., Selvaraj, K. and Kao, S.-J. (2012) Reconstruction of environmental changes using a multi-proxy approach in the Ulleung Basin (Sea of Japan) over the last 48 ka. *J. Quat. Sci.* **27**, 891–900.

Supplementary Materials

URL (http://www.terrapub.co.jp/journals/GJ/archives/data/54/MS606.zip)
Figures S1 to S3
Tables S1 to S3